Low Density Lipoprotein Aged in Plasma Forms Clusters Resembling Subendothelial Droplets: Aggregation via Surface Sites

Marco De Spirito,* Roberto Brunelli,[†] Giampiero Mei,[‡] Francesca R. Bertani,[§] Gabriele Ciasca,* Giulia Greco,[§] Massimiliano Papi,* Giuseppe Arcovito,* Fulvio Ursini,** and Tiziana Parasassi[§]

*Istituto di Fisica, Facoltà di Medicina e Chirurgia, Università Cattolica del Sacro Cuore, Rome, Italy; [†]Dipartimento di Scienze Ginecologiche, Perinatologia e Puericultura, Università di Roma "La Sapienza", Rome, Italy; [‡]Dipartimento di Medicina Sperimentale e Scienze Biochimiche, Università di Roma "Tor Vergata", Rome, Italy; [§]Istituto di Neurobiologia e Medicina Molecolare, Consiglio Nazionale delle Ricerche, Rome, Italy; and **Dipartimento di Chimica Biologica, Università di Padova, Padua, Italy

ABSTRACT   In early phases of atherogenesis, droplets and vesicles accumulate in the subendothelial extracellular space of arterial intima. There is much evidence to suggest that these droplets, ranging between 100 and 400 nm, derive from modified low-density lipoprotein (LDL). In investigations of the formation mechanism of these droplets, LDL fusion was previously induced in vitro by proteolysis, lipolysis, oxidation, and vigorous shaking, but all treatments failed to reproduce the size distribution range of in vivo droplets, mostly resulting, instead, in particles with a diameter intermediate between that of one and two LDL. Our approach was meant to mimic LDL aging in plasma. LDL isolated from plasma that was incubated overnight at 37°C is slightly modified in the secondary structure of its protein component and is primed to form very large aggregates according to a reaction-limited mechanism. This mechanism requires interactions between selected surface sites, whereas massive fusion is ruled out. In the frame of the general theory for colloids, the aggregation of LDL aged in plasma fulfills all the requirements of the reaction-limited mechanism, encompassing 1), exponential growth; 2), fractal structure, with the dimension of elementary constituent still consistent with a single LDL; and 3), extreme polydispersity of aggregates, with shape and dimension very close to that of droplets observed in vivo.

INTRODUCTION

Subendothelial retention of lipoprotein aggregates, in the form of droplets and vesicles, represents the commonly accepted paradigmatic early step in atherogenesis (1). Droplets and vesicles display features suggesting their origin from plasma low density lipoprotein (LDL) (2,3), such as 1), the presence of the apoprotein apoB-100; 2), a diameter between 100 and 400 nm, smaller than that of cytoplasmic cholesteryl ester droplets in foam cells; and 3), a fatty acid pattern of cholesteryl esters close to that of circulating lipoproteins. Furthermore, accumulation of extracellular droplets can be experimentally reproduced in rabbit arterial intima, in vivo, by injection of a large amount of human LDL (4).

The increased adhesion to subendothelial proteoglycans of LDL (2,5), the structure of which has been modified, is generally accepted as accounting for subendothelial retention, aggregate formation, and, therefore, the onset and progression of atherosclerotic lesions.

Proteolytic and lipolytic enzymes and oxidation have been used in searching for mechanisms in LDL modification able to promote aggregation and subendothelial retention. Nev-

ertheless, all these in vitro systems have failed to generate the size distribution of extracellular droplets observed in vivo. Actually, in the vast majority of results, the modification of LDL generated particles smaller than the sum of two LDL, therefore indicating a fusion process (2,3,6,7) rather than aggregation.

On the other hand, during their intravascular lifetime, from synthesis to removal, LDL particles are continuously remodeled, giving rise to subfractions heterogeneous in terms of apoB-100 structure and conformation (8,9), epitope expression (9–12), accessibility of protease sensitive sites (13,14), and affinity for the LDL receptor (9,15).

In this study, to partly model intravascular LDL aging, we incubated plasma at 37°C for ~20 h before LDL isolation and we obtained particles prone to spontaneously aggregate (LDLI). In LDLI, the only detectable difference from LDL isolated from fresh plasma was a decrease in the relative content of α-helix structure of apoB. LDLI aggregation occurs in the framework of a reaction-limited cluster aggregation (RLCA) mechanism, involving interactions between specific surface sites. Static and dynamic light scattering and atomic force microscopy (AFM) showed that LDLI clusters had shape and dimension quite similar to droplets and vesicles observed in vivo in atherosclerotic lesions. The characterization of LDLI aggregates according to the general RLCA mechanism gave both a structure and formation kinetics quite different from that extensively reported for in vitro modified LDL, thus suggesting novel approaches for the study of early atherogenesis.

MATERIALS AND METHODS

Isolation of lipoproteins

Venous blood was collected from healthy adult volunteers after overnight fasting, into Na_2EDTA-Vacutainer tubes and centrifuged at $1,500 \times g$ for 10 min at 4°C. Plasma was either immediately used for LDL isolation (LDLF) or incubated in a cell culture incubator in capped sterile tubes for ~20 h at 37°C before LDL isolation (LDLI). LDL was isolated by two utracentrifugation runs at $540,000 \times g$ at 4°C for 4 h, first in saline solution A (0.2 M NaCl, 0.2 mM EDTA, pH 7.4, $\delta = 1.0063$ g/ml), then in saline solution B (solution A adjusted to $\delta = 1.063$ g/ml with KBr). The floating layer after the second centrifugation contained the isolated LDL fraction. The yield of LDLF and LDLI from the same plasma was always practically identical. The isolated LDL was routinely tested by SDS gradient (4–15%) polyacrylamide gel electrophoresis under nonreducing conditions and stained with Comassie brilliant blue. No fragmentation or difference in apoB-100 migration was observed. After overnight dialysis in phosphate saline buffer, pH 7.4, LDL was used for light scattering measurements. LDL oxidative modification was carried out by adding 50 μM $CuSO_4$ to 1 μM LDL (calculated as apoB-100 content), at the beginning of light scattering measurements.

Light scattering measurements

LDL, at protein concentrations of 1 mg/ml, were used for measurements by using a commercial light scattering set-up ALV spectrometer (ALV, Langen, Germany) consisting of a CGS-5000 rotating arm goniometer, a photomultiplier tube (PMT) (EMI, Ruislip, UK), an ALV 5000 multi-tau digital correlator operating with a sampling time of 200 ns, and an Innova 70 argon ion laser (Coherent, Santa Clara, CA) operated at 488 nm and 100 mW. The scattering cell was immersed in a refractive index matching fluid (toluene) kept at 37 ± 0.1°C. Static and dynamic light scattering data were collected simultaneously from a scattering volume of ~100 μm^3, and analyzed with homemade software. Angular runs were performed with angles logarithmically scaled in $sin(\theta)$, where θ is the scattering angle, ranging from 30° to 150°. For each angle, data were typically acquired for 5 min.

Atomic force microscopy measurements

AFM imaging was performed by an SPMagic SX atomic force microscope (Elbatech, Italy) in the tapping operation mode; ~50 μl of LDL suspension was smeared over a glass coverslip, dehydrated under a mild nitrogen flow, washed with pure water to remove salt crystals, and imaged. The microscope probe consisted of an ultrasharp silicon nitride cantilever of nominal force constant $k = 40$ N/m with a tip radius of <10 nm (MikroMash, Tallinn, Estonia). Image analysis was performed by a WSxM software (Nanotec Electrónica, Madrid, Spain).

Fitting experimental data to the general aggregation theory

The complete description of a cluster aggregation process requires the determination of the cluster structure, of the aggregation kinetics, and of the cluster-mass distribution function (16).

The structure of a fractal aggregate is characterized by a self-similarity symmetry upon change of length scale described by a power law relating the mass, M, and the cluster radius, r : $M \propto r^{d_f}$. By describing the spatial distribution of the elementary aggregating particle into the cluster, the fractal dimension, d_f, defines the cluster structure (17). The d_f value is typically lower than the Euclidean dimension $d_f = 3$. Because of the random nature of the process, the dynamics of aggregation is described on a statistical basis by monitoring the time evolution of the cluster-mass distribution function $N(M)$

(18). Therefore, the aggregation rate is measured by the growth in time of the average cluster mass:

$$\overline{M} = \sum_M N(M)M^2 / \sum_M N(M)M, \qquad (1)$$

where $\sum_M N(M)M$ is the number of the elementary aggregating particles.

Two regimens of aggregation kinetics have been observed and theoretically described (19), both determined by the short-range interparticle interactions that affect the sticking probability, p, of two colliding particles. Each of these two regimens is characterized by a different time evolution of the average cluster mass, $\overline{M}$, the shape of cluster-mass distribution function, and the fractal dimension of the resulting clusters. These parameters are strictly interconnected and related to the mechanisms that drive the aggregation kinetics (20). The first mechanism, named diffusion-limited cluster aggregation (DLCA), results in a rapid aggregation and occurs when two particles stick together after each collision ($p = 1$). In this case, the aggregation rate is solely dependent on the time between two collisions, and clusters are essentially monodisperse in that their mass distribution is bell-shaped and peaked around an average mass value, which grows linearly with time. For DLCA, computer simulation and several different experimental techniques obtained a typical fractal dimension $d_f = 1.8$. The second regimen, on the other hand, the RLCA, occurs when several collisions are required before two particles can stick together ($p < 1$). In this slow aggregation regimen, clusters have a structure more dense than in the DLCA, and with a typical d_f of 2.1. The average cluster mass is an exponential function of time, $\overline{M} \propto e^{At}$, where A is a constant that depends on the sticking probability and on the time between collisions. Clusters formed in the RLCA regimen show an extremely high mass polydispersity, described by a power law, up to a cutoff mass M_c, after which it decreases exponentially according to

$$N(M) = M^{-\tau_P} e^{-M/M_c}, \qquad (2)$$

where $\tau_P = 1.5$ is a characteristic exponent (19,21).

The DLCA and RLCA regimens must be considered universal in that their features do not depend on the nature of interacting forces between particles.

Spectroscopy and microscopy techniques usually detect the normalized number-weighted radius distribution function, $p_N(r)$, instead of the cluster-mass distribution function, $N(M)$. For a direct comparison of the theoretical predictions with experimental results, we here developed the relation between these two distributions. By definition, $p_N(r) = N(r)/N$, where $N(r)$ is the number of clusters of radius r and N is the total number of clusters ($N = \int N(r)dr$). Since $N = \int N(M)dM$, for fractal clusters we obtain $N(r) \propto N(M)r^{d_f-1}$. In the case of RLCA aggregation, we obtain

$$p_N(r) \propto r^{-[d_f(\tau-1)+1]} e^{-(r/r_c)^{d_f}}, \qquad (3)$$

where r_c is the cut-off radius of clusters with a mass M_c.

Light scattering data analysis

Static light scattering (22) measures the time-averaged Rayleigh ratio, $R(q)$, i.e., the normalized power scattered as a function of the scattering wave vector $q = (4\pi n/\lambda)sin(\theta/2)$, where θ is the scattering angle, λ is the laser wavelength, and n the refractive index. For a polydisperse sample with a continuous mass distribution, $R(q)$ can be expressed as (22)

$$R(q) = K_c \frac{\sum_M N(M)M^2 S(qr)}{\sum_M N(M)M}, \qquad (4)$$

where K is the optical constant given by $K = (4\pi^2/\lambda^4 N_A)n^2(\partial n/\partial c)^2$, with N_A being the Avogadro number, c the sample concentration (g/ml), $(\partial n/\partial c)$ the refractive index increment of the solute (ml/g), M the particle molar weight (g), and $S(qr)$ the structure factor. In fractal aggregates, the structure factor $S(qr)$ can be obtained analytically by Fourier-transforming the

pair-correlation function of fractal spherical objects (23). Its form normalized to $S(0) = 1$ is given by

$$S(qr) = \frac{\sin[(d_f - 1)arctg(qr)]}{(d_f - 1)qr(1 + q^2r^2)^{d_f - 1/2}}, \quad (5)$$

where the $S(qr)$ dependence on the product qr follows the scale invariance of the cluster. Two asymptotic behaviors of the structure factor can be found during aggregation:

$$S(qr) = \begin{cases} 1 & qr \gg 1 \\ (qr)^{-d_f} & qr \ll 1 \end{cases}. \quad (6)$$

When clusters can be considered as point sources, i.e., $qr \ll 1$, the Rayleigh ratio can be used to determine the time evolution of the average cluster masses: $R(q) \propto \sum_M N(M)M^2 \propto M$. When clusters are large enough and most of them have $qr \gg 1$, the fractal dimension d_f can be directly determined by measuring the slope of the Rayleigh ratio versus the wave vector q distribution: $R(q) \propto q^{-d_f}$. In the crossover region of $qr \sim 1$, the full expression (Eq. 3) must be used.

Dynamic light scattering (DLS) (24) provides additional information on the aggregation kinetics and on the cluster dimension and evolution as the aggregation proceeds. The DLS technique measures the intensity autocorrelation function $g_2(\tau) = \langle I(t)I(t+\tau)\rangle/\langle I\rangle^2$, where τ is the lag time and brackets represent the ensemble average. The $g_2(\tau)$ can be related to the field autocorrelation function $g_1(\tau)$ through the Siegert relation $g_2(\tau) = 1 + g_1^2\beta(\tau)$, where β is an instrumental constant (in our set-up, $\beta = 1$). The mathematical form of $g_1(\tau)$ depends on the physical properties of the investigated system. For monodisperse particles, the density correlation function decays exponentially according to $g_1(\tau) = e^{-\Gamma\tau}$, where the decay rate Γ depends on the particle translational diffusion coefficient according to $\Gamma = Dq^2$. For a polydisperse sample, $g_1(\tau)$ is more complex than a single exponential. In this case the distribution of decay rates must be accounted for by introducing a weighting function (24),

$$g_1(\tau) = \int_0^\infty p_I(r_h)e^{-\Gamma(r_h)\tau}dr_h, \quad (7)$$

where $p_I(r_h)$ is the normalized intensity-weighted radius distribution function describing the distribution of the fraction of the intensity scattered by a particle of hydrodynamic radius r_h and decay rate $\Gamma(r_h)$, given by

$$\Gamma(r_h) = kTq^2/6\pi\eta r_h, \quad (8)$$

where η is the water viscosity and k the Boltzman constant.

The recovery of the $p_I(r_h)$ distribution, a classical hill posed problem, can be obtained by the regularized Laplace inversion of the intensity autocorrelation function (25,26). In this case, the intensity-weighted radius distribution is obtained by a direct numerical inversion of the DLS data. In the presence of highly polydisperse fractal clusters, we also have to account for the volume and for the inner structure of clusters, so we need a complete recovery of the normalized number-weighted radius distribution function $p_N(r_h)$ (27):

$$p_N(r_h) = p_I(r_h)/(S(qr_h)M^2(r_h)), \quad (9)$$

where $M(r_h)$ is the mass of a cluster of radius r_h. Finally, once $p_N(r_h)$ is known, the mean hydrodynamic radius can be easily determined by

$$\langle r_h \rangle_N = \int_0^\infty p_N(r_h)r_h dr_h. \quad (10)$$

Circular dichroism

Circular dichroism (CD) spectra of 0.1 μM LDL samples (calculated as apoB-100 content) were recorded on a JASCO spectropolarimeter (Tokyo, Japan),

using a 0.1-cm quartz cuvette, in the peptidic region (200–250 nm). To increase the signal/noise ratio, six spectra were averaged for each measurement. The cell holder compartment was maintained at 37 ± 0.1°C by a circulating water bath. The spectra were analyzed for their content in secondary structure by using the software accompanying the spectropolarimeter.

RESULTS

Oxidatively modified LDL undergoes a fusion process

According to previous literature, Cu^{2+}-induced oxidative modification affects both the protein and lipid component of LDL, resulting in aggregation and fusion, where aggregation indicates the sticking between two particles that precedes fusion (2). We confirmed these results by adding $CuSO_4$ to LDL (OxLDLF) at the beginning of light scattering measurements, and comparing the results to those obtained from LDL isolated immediately after the blood collection (LDLF). Particle size was determined by static light scattering measurements at $\theta = 30$°. In particular, the Rayleigh ratio, $R(q)$, which is directly related to the volume of particles (Eq. 4), was measured as a function of time and reported in Fig. 1 a. For OxLDLF, the $R(q)$ showed a sudden increase in a few hours ($\sim$5 h), then reached a constant value, about twice the initial one. The initial $R(q)$ value of LDLF was similar to that of OxLDLF and remained constant up to $\sim$20 h, when it slowly increased to an asymptotic value close to that of OxLDLF.

To better characterize the extent of the aggregation process, we also performed dynamic light scattering experiments by measuring the intensity autocorrelation function. The time evolution of the average hydrodynamic radius of the clusters, $\langle r_h \rangle_N$, was determined (Eq. 10). The results for both LDLF and OxLDLF are reported in Fig. 1 b. Again, after a rapid increase, the $\langle r_h \rangle_N$ of OxLDLF reached a constant value (17 $\pm$ 1 nm), larger than the initial hydrodynamic radius of LDLF ($\langle r_{h0} \rangle_N = 11.3 \pm 0.2$ nm), but smaller than that of the sum of two particles. As for LDLF, an asymptotic value close to that observed for OxLDLF was obtained, but, consistently with the static light scattering data, after a longer time ($\sim$20 h). The behavior of LDLF can be accounted for by a slow oxidation, as described for the so-called minimally modified LDL (28). On the whole, the hydrodynamic radii of OxLDLF and LDLF confirm a fusion process driven by a Cu^{2+}-catalyzed (2,3,6,7) or a noncatalyzed (28) oxidative modification.

LDL isolated from plasma previously incubated at 37°C undergoes a reaction-limited aggregation process

In striking contrast with the results reported in Fig. 1, a different aggregation mechanism characterizes LDL separated from plasma that was previously incubated for $\sim$20 h at 37°C (LDLI). After a lag phase, both static and dynamic light
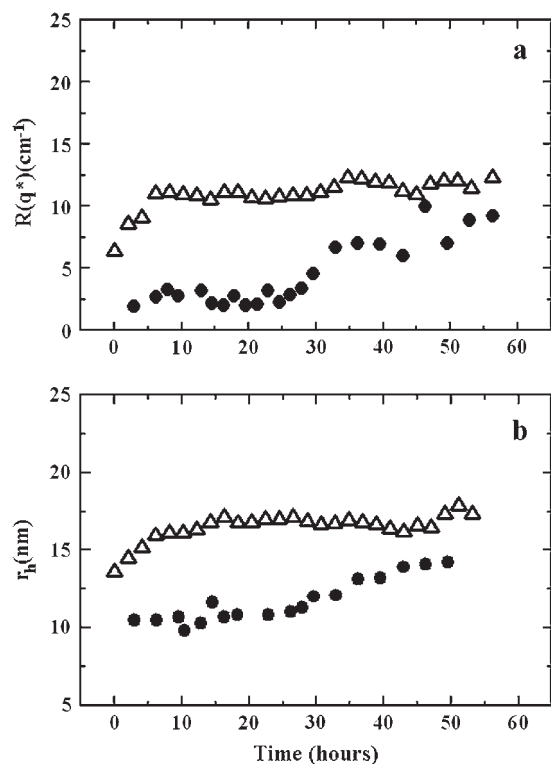
FIGURE 1 Time evolution of the Rayleigh ratio (*a*) and of the hydrodynamic radius (*b*) for oxidatively modified LDL. The $R(q*)$ value was collected at $\theta = 30°$ for LDL isolated from fresh plasma (LDLF) (●) and LDLF in the presence of Cu^{2+} (OxLDLF; molar ratio apoB-100/Cu^{2+} = 1:50) (△). Measurements were made at 37°C.

FIGURE 2 Time evolution of the Rayleigh ratio (*a*) and of the hydrodynamic radius (*b*) during LDLI aggregation. The $R(q*)$ value was collected at $\theta = 30°$ for LDL isolated after plasma incubation at 37°C for ~20 h (LDLI) (○). The exponential increase is evidenced by the solid line. To facilitate comparison, in both panels the behavior of LDL isolated from fresh plasma (LDLF) (●) is also reproduced. Measurements were made at 37°C.

scattering data (Fig. 2) showed an impressive, exponential, increase of the Rayleigh ratio, $R(q)$, and of the hydrodynamic radius, $\langle r_h \rangle_N$, the latter reaching a plateau at a value of ~200 nm, at ~36 h. For this LDLI sample, the fit of experimental data to $\langle r_h \rangle_N = \langle r_{h0} \rangle_N e^{-k(t-t_a)}$ gave for the rate constant a value $k = (24 \pm 2)$ h^{-1} and for the lag phase a value $t_a = (21.7 \pm 0.3)$ h.

For LDLI, the time evolution of both $R(q)$ and $\langle r_h \rangle_N$ is consistent with the theoretical predictions for clusters undergoing an RLCA mechanism. We therefore verified in detail all other theoretical predictions of RLCA, i.e., the inner structure of aggregates, given by the fractal dimension d_f, and their mass distribution.

Given $M \propto r^{d_f}$, the fractal dimension can in principle be determined by the slope in the log-log plot of the cluster mean mass versus the cluster radius r. M and r are quantities experimentally hard to obtain. Nevertheless, when probing dimensions smaller than the cluster radius ($qr \gg 1$ in Eq. 6) and according to Eq. 4, a direct proportionality between M and the Rayleigh ratio $R(q)$ results. Therefore, in the case of fractal aggregates, the plot of $R(q)$ versus q (by definition proportional to r^{-1}) is a power law with exponent -d_f. In Fig. 3, we report the distribution of $R(q)$ versus q for the LDLI sample at the end of the aggregation process. The linear
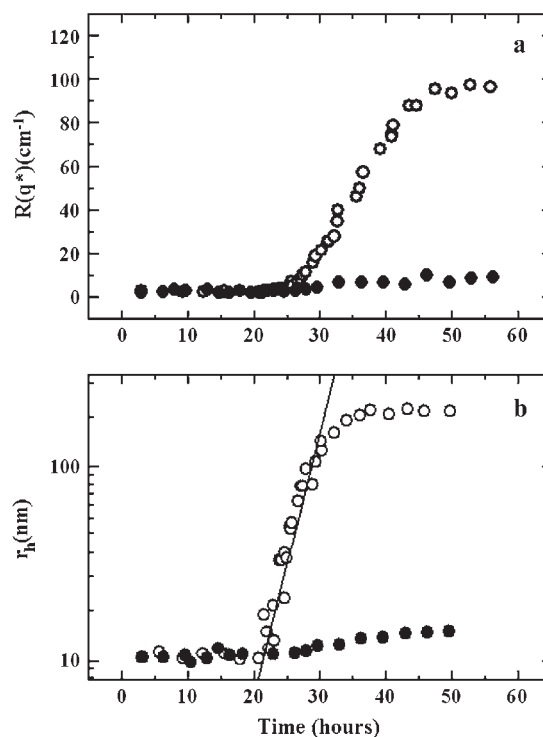
behavior of the log-log plot shows that the distribution of the cluster structure factor approaches a power law, as expected from fractal aggregates of very large size (Eq. 6). By fitting Eq. 6 to the experimental data, we obtained a value of the fractal dimension $d_f = 2.1 \pm 0.2$, well in agreement with that expected for a collection of fractal clusters undergoing an RLCA aggregation (18,19). Alternatively, the fractal dimension of the cluster can also be obtained from $R(q)$ relative to the average hydrodynamic radius. From Eqs. 4, 6, and 8, the following relation must hold (18):

$$R(q) \propto \langle r_h \rangle^{d_f}. \qquad (11)$$

When plotted versus $\langle r_h \rangle_N$ in a log-log scale (Fig. 3, *inset*), $R(q)$ well fits a power law from which the value of the fractal dimension was again calculated, yielding $d_f = 2.1 \pm 0.3$, in excellent agreement with the value obtained above.

The shape of the cluster-mass distribution provides further fundamental information that helps in characterizing the aggregation mechanism. Because of the limited width of this distribution, in some cases, static light scattering cannot provide a determination of the shape of the cluster-mass distribution (29). A different strategy consists in the recovery of the cluster-radius distribution, $p_N(r_h)$, directly from the
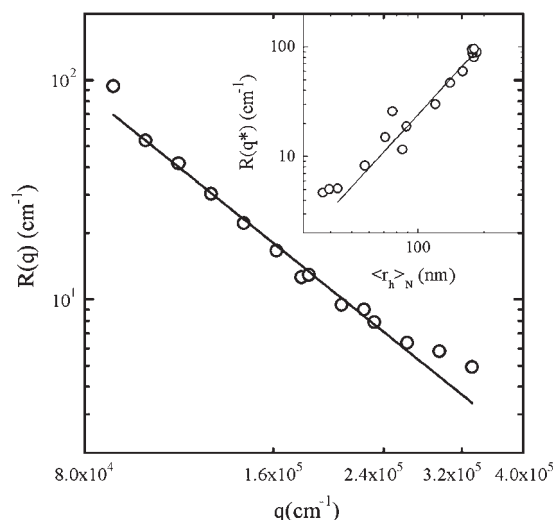
FIGURE 3 Log-log plot of the scattered $R(q)$ distributions as a function of the wave vector q for the LDLI sample at the plateau ($t = 9 \times 10^5$ s). The solid line represents the best fit of the data following Eqs. 4 and 6, from which the fractal dimension $d_f = 2.1 \pm 0.02$ has been determined. (*Inset*) $R(q*)$ (where $q*$ denotes measurements performed at $\theta = 30°$) is plotted versus $\langle r_h \rangle_N$. The best data fit (Eq. 11) (*solid line*) gave the value $d_f = 2.1 \pm 0.2$.

intensity autocorrelation function (27). In Fig. 4 *a*, we report four different representative distributions of $p_N(r_h)$ taken at different times during LDLI aggregation. As expected, radius distributions shift toward higher values with time, and, more relevant, all distributions appear broad and highly asymmetric. In Fig. 4 *b*, Eq. 5 was fitted to radius distributions and reported in a log-log plot for different times during LDLI aggregation. Fitting parameters are reported in Table 1. In agreement with the RLCA aggregation theory, all curves show a decay well described by a power law, $P_n(r_h) \propto r_h^{-\delta}$, with $\delta = d_f(\tau - 1) + 1$, up to a cut-off radius, r_c, after which an exponential decay is observed (Eq. 3). Notably, the fractal dimension does not vary as aggregation proceeds, keeping a constant value of 2.1 ± 0.9.

Atomic force microscopy confirms light scattering results

Some of the above findings were further confirmed by AFM observations, whose analysis does not require an ab initio model.

In Fig. 5 *a*, we report a representative AFM image of LDLI at the end of the aggregation process ($t \sim 50$ h). The number-weighted particle size distribution, calculated over three images, is reported in Fig. 5 *b*, together with the cluster-radius distribution, $p_N(r_h)$, calculated by DLS. It is noteworthy that despite the perturbative method needed to prepare the AFM samples, the particle size distributions obtained from AFM images perfectly overlap those obtained by DLS, giving further support to the analysis method that we developed.
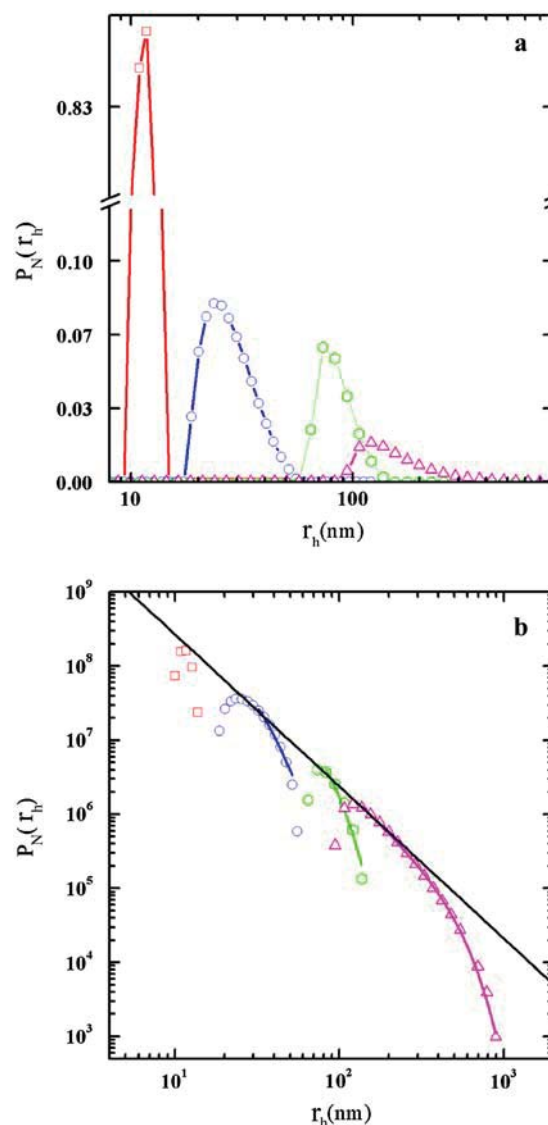

FIGURE 4 (*a*) Semilog plot of the cluster-radius distributions taken at different times as the aggregation evolves (namely, $t = 10^2$ s (*red squares*), 10^3 s (*blue circles*), 10^4 s (*green circles*), and 7×10^5 s (*violet triangles*)). All distributions appear highly asymmetric, with increasing asymmetry at higher $\langle r_h \rangle_N$ values. (*b*) log-log plot of $p_N(r_h)$ versus $\langle r_h \rangle_N$ at different times as the aggregation proceeds, using the same symbols and colors as in *a*. Also reported is the best fit of the data to Eq. 5 (*black line*).

## LDLI shows a modified secondary structure

Possible reasons for the propensity of LDLI to aggregation were investigated by analyzing the secondary structure of its protein component. Circular dichroism spectra of isolated LDLI ($t = 0$) showed a decreased absorbance with respect to LDLF of $\sim 20\%$ at 220 nm (Fig. 6 *a*). Such a structural change did not show further modifications during the aggregation process, up to 48 h (Fig. 6 *b*). In the limits of available analysis modeling, from LDLI spectra we obtained a relative increase in the β-sheet content paralleled by a relative decrease in the α-helix structure. In quantitative

TABLE 1 Results of structure-factor fits of DLS data taken at different times during aggregation

t_s (s)	τ_p	d_f	r_c (nm)
10^2	1.5	2.15	41 ± 6
10^3	1.5	2.15	83 ± 27
10^4	1.48 ± 0.02	2.15	520 ± 100
7×10^5	1.48 ± 0.6	2.15 ± 0.9	523 ± 640

For a discussion of the structure factor, see text and Eq. 5. Note that although the cutoff radius (r_c) increases during aggregation, the characteristic exponent τ_p and the fractal dimension d_f remain constant, with values well in agreement with theoretical predictions.

terms, the β-sheet structure increased to $8 \pm 2\%$, whereas the α-helix structure decreased to $18 \pm 7\%$. OxLDLF showed quite a different behavior in the time evolution of CD spectra. Consistently with reported CD data (30), OxLDLF showed a sudden decrease in the CD absorbance, with a loss of ~44% at 220 nm in <50 min (Fig. 6 b). This decrease indicates a more severe alteration in the particle's structure than that occurring during LDL aging in plasma. Indeed,
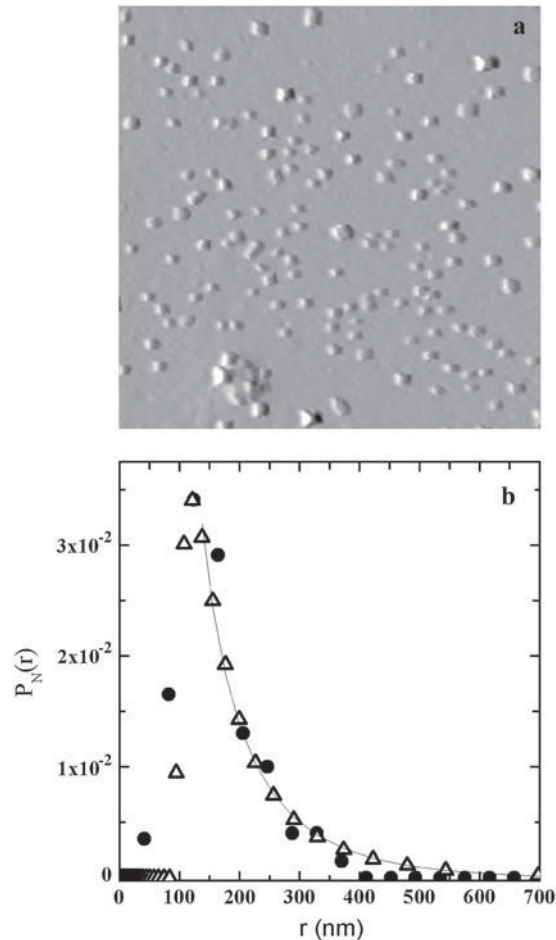
FIGURE 5 (*a*) Representative AFM image of LDLI at the end of the aggregation ($t \sim 50$ h). Frame of 16×16 μm. (*b*) Number-weighted particle size distribution of LDLI calculated over three AFM images (●) and calculated from the light scattering data (△).

such a strong structural loss in <1 h renders questionable an analysis of CD spectra in terms of β-sheet and α-helix content. The fast structural change in OxLDLF is in agreement with the rapid particle fusion observed by light scattering (Fig. 1).

DISCUSSION

Previous in vitro studies on LDL after treatment with proteases, lipases, or oxidative agents (2), or after vortexing (31), reported the occurrence of aggregation and fusion. Fusion was observed 1), after an extensive fragmentation of apoB-100 by α-chymotripsin for 24 h, resulting in a mean particle diameter of 37 ± 8.5 nm (3); 2), after a substantial proportion of sphingomyelin was hydrolyzed by sphingo-myelinase, resulting in 35% of the particles with a diameter larger than that of native LDL (7); 3), after ~30% of phosphatidylcholine was hydrolyzed by secretory phospho-lipaseA2, resulting in an average particle diameter of 32 nm (6); and 4), after a 16-h incubation with three different cathepsins, resulting in particles always smaller than the sum of two LDL (32). Aggregation was observed after treatment with phospholipaseA2, and aggregates consisted of particles with a diameter smaller than that of native LDL, i.e., <18 nm (33). In addition to these LDL modifications, affecting either the protein or the lipid component of the LDL particle, Cu^{2+}-induced oxidative modification of LDL was reported to modify both components, resulting in aggregation and fusion (2), thus modeling different LDL modifications. Overall, previous literature on LDL aggregation/fusion demonstrated that extensive in vitro proteolysis, lipolysis, or oxidative modification generates fused LDL particles with a diameter of less than twice that of native LDL.

We reproduced the above findings by using Cu^{2+}-modified LDL. This treatment has been reported to affect both the protein and the lipid components in LDL, and to induce both aggregation and fusion, where the term aggregation refers to the sticking between two particles that precedes fusion (2). Our DLS measurements confirmed the occurrence of fusion in OxLDLF, resulting in particles with a hydrodynamic radius of $\langle r_h \rangle_N = 17 \pm 1$ nm. Therefore, in our experiments, a profound in vitro oxidative modification of LDL also generates fusion.

LDL separated from plasma that was previously incubated at 37°C (LDLI) showed no evidence of fusion, but an impressive aggregation process quite different from that observed after oxidative modification. To characterize the LDLI aggregation mechanism we used a data analysis procedure in the frame of the general theory for the description of colloid aggregation (18,19,29), that allows the recovery of the mean particle radius and of the entire particle size distribution even by a single-angle DLS intensity autocorrelation function (27). We conclusively proved that these LDLI samples aggregate according to an RLCA mode, which implies quite a different mechanism of
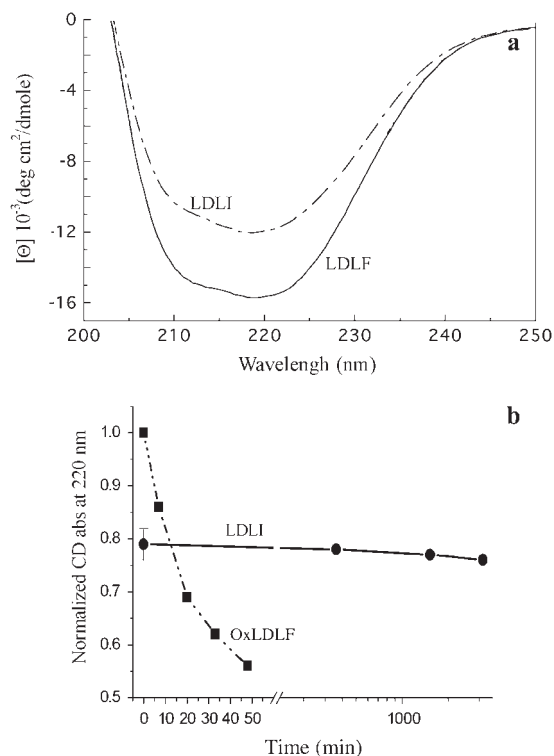
FIGURE 6 Secondary structure of the protein component in the different LDL samples. (*a*) Representative CD spectra of LDLF and LDLI at $t = 0$. (*b*) Normalized CD absorbance at 220 nm as a function of time in OxLDLF and in LDLI. The values for the LDLI sample were normalized to the LDLF absorbance. For plot readability, after the break the *x* axis is logarithmically spaced.

interaction than that previously outlined. Indeed, in RLCA, aggregation depends on the sticking between specific surface sites (sticking probability <1) and results in 1), a lag phase followed by an exponential increase of the mean radius; 2), a broad size distribution of aggregates; and 3), a fractal dimension $d_f = 2.1$ of formed clusters.

Again in agreement with the RLCA mechanism of aggregation, the exponential increase of particle radius with time indicates that, together with cluster-monomer, LDL aggregation also occurs through cluster-cluster interactions (29). Indeed, clusters with larger size and more potential surface bonding sites grow faster than smaller ones. Consistent with the RLCA regimen, the lag phase represents the initial particle nucleation. In the formed clusters, the radius of the unit constituting aggregates, $\langle r_{h0}\rangle_N = 11.3 \pm 0.2$ nm, still corresponds to the single LDL (34,35). This last $\langle r_{h0}\rangle_N$ value was also the starting value for both LDLF and LDLI, indicating that plasma incubation did not affect LDL size.

Notably, the broad particle-size distributions, calculated from AFM and DLS data, perfectly overlap. In addition, the recovered size distribution of LDLI aggregates closely resembles that of extracellular droplets and vesicles visualized in atheromatous lesions, in the range 100–400 nm (2).

The fractal dimension of LDL clusters was determined using four different approaches: 1), static light scattering,

through the evaluation of the structure factor $S(q,r)$ from the $R(q)$ distribution (Eqs. 4 and 6); 2), static and dynamic light scattering, by comparing the $R(q)$ distribution with the average hydrodynamic radius (Eq. 11); 3), by fitting Eq. 3 to the normalized number-weighted radius distribution obtained by DLS measurements; and 4), by fitting Eq. 3 to the $p_N(r)$ values measured by AFM. We note that Eq. 3 is generally valid for the RLCA type of aggregation and therefore could be applied to the analysis of data acquired by different techniques. Indeed, in our case, Eq. 3 has been used to analyze both spectroscopy (DLS) and microscopy (AFM) data giving identical results in the determination of $d_f = 2.1$. The existence of such a fractal dimension, consistently supported by all our results, and constant over all the aggregation process, constitutes a relevant finding. As an immediate consequence, it contradicts the notion that clusters of LDLI formed upon aggregation are due to fusion, contrary to what was previously reported after in vitro LDL treatments. In the LDLI case, instead, cavities are present in clusters, and their elementary constituent maintains its individuality.

With respect to previously reported data (2,3,5–7,31–33), distinctive features of our results on the mechanism of LDL aggregate formation are 1), the need for a surface interaction between specific sites; 2), the absence of fusion; and 3), the generation of the complete size distribution of lipid droplets evidenced in vivo. Although proteases, lipases, and oxidants are certainly present in the circulating blood, clearly the whole biological complexity is not fully modeled by isolated elements and by highly perturbative experimental procedures.

The observation that LDLI aggregates through a mechanism quite different from that of OxLDLF stimulates the question of the reason for LDLI's propensity to aggregation. The observation of a decreased CD absorbance in the LDLI protein component suggests an explanation. A subtle modification of apoB-100 secondary structure, with a relative increase in potentially sticky β-sheet structures, occurs during plasma incubation. Although the origin of this change in apoB-100 structure during the plasma incubation still needs to be clarified, it may well represent a spontaneous structural rearrangement. The new protein secondary structure in LDLI is indeed stable, as revealed by its constant CD absorbance during aggregation. Severe proteolytic or lipolytic modifications in LDLI can be excluded for the lack of gross protein fragmentation and for the value of its hydrodynamic radius, quite similar to that of LDLF. On the contrary, a severe modification of CD absorbance was detected in OxLDLF shortly after the addition of the catalyst Cu^{2+}, again supporting the notion that severe in vitro perturbative procedures fail to mimic physiological processes.

CONCLUSIONS

Different from oxidatively modified LDL, LDL isolated from plasma that was previously incubated at 37°C spontaneously aggregates through a mechanism leading to clusters

that mimic the shape and size distribution of droplets and vesicles observed in atheromatous lesions. The formed clusters are not constituted by fused LDL.

Aggregation of LDL occurs through a reaction-limited process, i.e., it involves specific sites on the particle's surface being characterized by a sticking probability <1. This represents a novel and different mechanism with regard to the previously reported fusion and indicates, instead, an aggregation mechanism driven by interactions between specific surface sites. A reaction-limited aggregation can originate from either collisions between a limited number of high-affinity sites or collisions between several sites of low affinity. After proteolytic or lipolytic treatment, the occurrence of LDL aggregation/fusion was explained by an increase in lipid hydrophobic sites, but the type of LDL aggregates produced remarkably differed from those described herein. Therefore, we do not have arguments to support the claimed relevance of lipidic domains as a driving force in cluster formation (7). Indeed, our results on the response of the fluorescent lipid probe laurdan (30) show minor differences between the LDLF and LDLI samples (not shown). Based on structural data, we suggest that the propensity to aggregation of LDLI has to be attributed to a mild modification in the secondary structure of the LDLI protein component, exposing sticky regions that still remain to be determined. On the contrary, as suggested by the severe structural loss, these aggregation-prone sites may be lost in OxLDLF, therefore promoting a hydrophobic interaction. Finally, the lag time before the exponential growth of aggregates is reasonably needed to reach a critical concentration of clusters, similar to nucleation processes. Intriguingly, both a lag phase and an exponential growth in cluster formation constitute landmarks in the aggregation process of misfolded proteins, which is involved in a variety of pathologies (36).

The possible occurrence and persistence of aggregation-prone particles in human blood can lead to additional perspectives in understanding the onset of vascular diseases. The availability of ex vivo LDL droplet-like aggregates, obtained as first described herein, represents an attractive tool for modeling the vascular response. Similarly, a further understanding on the origin of aggregation-prone LDL might open prevention and therapeutic possibilities.

REFERENCES

1. Skålén, K., M. Gustafsson, E. Knutsen Rydberg, L. Mattsson Hultén, O. Wiklund, T. L. Innerarity, and J. Borén. 2002. Subendothelial retention of atherogenic lipoproteins in early atherosclerosis. *Nature.* 417:750–754.

2. Öörni, K., M. O. Pentikäinen, M. Ala-Korpela, and P. T. Kovanen. 2000. Aggregation, fusion, and vesicle formation of modified low density lipoprotein particles: molecular mechanisms and effects on matrix interactions. *J. Lipid Res.* 41:1703–1714.

3. Piha, M., L. Lindstedt, and P. T. Kovanen. 1995. Fusion of proteolyzed low-density lipoprotein in the fluid phase: a novel mechanism generating atherogenic lipoprotein particles. *Biochemistry.* 34:10120–10129.

4. Nievelstein, P. F., A. M. Fogelman, G. Mottino, and J. S. Frank. 1991. Lipid accumulation in rabbit aortic intima 2 hours after bolus infusion of low density lipoprotein. A deep-etch and immunolocalization study of ultrarapidly frozen tissue. *Arterioscler. Thromb.* 11:1795–1805.

5. Pentikäinen, M. O., E. M. P. Lehtonenm, K. Öörni, S. Lusa, P. Somerharju, M. Jauhiainen, and P. T. Kovanen. 1997. Human arterial proteoglycans increase the rate of proteolytic fusion of low density lipoprotein particles. *J. Biol. Chem.* 272:25283–25288.

6. Hakala, J. K., K. Öörni, M. O. Pentikäinen, E. Hurt-Camejo, and P. T. Kovanen. 2001. Lipolysis of LDL by human secretory phospholipase A(2) induces particle fusion and enhances the retention of LDL to human aortic proteoglycans. *Arterioscler. Thromb. Vasc. Biol.* 21: 1053–1058.

7. Öörni, K., J. K. Hakala, A. Annila, M. Ala-Korpela, and P. T. Kovanen. 1998. Sphingomyelinase induces aggregation and fusion, but phospholipase A2 only aggregation, of low density lipoprotein (LDL) particles. *J. Biol. Chem.* 273:29127–29134.

8. McNamara, J. R., D. M. Small, Z. Li, and E. J. Schaefer. 1996. Differences in LDL subspecies involve alterations in lipid composition and conformational changes in apolipoprotein B. *J. Lipid Res.* 37:1924–1935.

9. Galeano, N. F., R. Milne, Y. L. Marcel, M. T. Walsh, E. Levy, T. D. Ngu'yen, A. Gleeson, Y. Arad, L. Witte, M. Al-Haideri, S. C. Rumsey, and R. J. Deckelbaum. 1994. Apoprotein B structure and receptor recognition of triglyceride-rich low density lipoprotein (LDL) is modified in small LDL but not in triglyceride-rich LDL of normal size. *J. Biol. Chem.* 269:511–519.

10. Tikkanen, M. J., T. G. Cole, K. S. Hahm, E. S. Krul, and G. Schonfeld. 1984. Expression of apolipoprotein B epitopes in very low density lipoprotein subfractions. Studies with monoclonal antibodies. *Arteriosclerosis.* 4:138–146.

11. Marcel, Y. L., M. Hogue, P. K. Weech, J. Davignon, and R. W. Milne. 1988. Expression of apolipoprotein B epitopes in lipoproteins. Relationship to conformation and function. *Arteriosclerosis.* 8:832–844.

12. Kinoshita, M., E. S. Krul, and G. Schonfeld. 1990. Modification of the core lipids of low density lipoproteins produces selective alterations in the expression of apoB-100 epitopes. *J. Lipid Res.* 31:701–708.

13. Chen, G. C., S. Zhu, D. A. Hardman, J. W. Schilling, K. Lau, and J. P. Kane. 1989. Structural domains of human apolipoprotein B-100. Differential accessibility to limited proteolysis of B-100 in low density and very low density lipoproteins. *J. Biol. Chem.* 264:14369–14375.

14. Chen, G. C., K. Lau, R. L. Hamilton, and J. P. Kane. 1991. Differences in local conformation in human apolipoprotein B-100 of plasma low density and very low density lipoproteins as identified by cathepsin D. *J. Biol. Chem.* 266:12581–12587.

15. Campos, H., K. S. Arnold, M. E. Balestra, T. L. Innerarity, and R. M. Krauss. 1996. Differences in receptor binding of LDL subfractions. *Arterioscler. Thromb. Vasc. Biol.* 16:794–801.

16. Weitz, D. A., M. Y. Lin, and J. S. Huang. 1987. Fractal and scaling in kinetic colloid aggregation. *In* Physics of Complex and Supermolecular Fluids. S. A. Safran and N. A. Dark, editors. Wiley-Interscience, New York. 509–545.

17. Mandelbrot, B. B. 1982. The Fractal Geometry of Nature. Freeman, San Francisco.

18. Weitz, D. A., and M. Oliveria. 1984. Fractal structures formed by kinetic aggregation of aqueous gold colloids. *Phys. Rev. Lett.* 52:1433–1436.

19. Lin, M. Y., H. M. Lindsay, D. A. Weitz, R. C. Ball, and R. Klein. 1989. Universality of fractal aggregates as probed by light scattering. *Proc. R. Soc. Lond. A.* 423:71–87.

20. Ball, R. C., D. A. Weitz, T. A. Witten, and F. Leyvraz. 1987. Universal kinetics in reaction-limited aggregation. *Phys. Rev. Lett.* 58:274–277.

21. Broide, M. L., and R. J. Cohen. 1990. Experimental evidence of dynamic scaling in colloidal aggregation. *Phys. Rev. Lett.* 64:2026–2029.

22. Kerker, M. 1969. The Scattering of Light and Other Electromagnetic Radiation. Academic Press, New York.

23. Chen, S. H., and J. Texteira. 1986. Structure and fractal dimension of protein-detergent complexes. *Phys. Rev. Lett.* 57:2583–2586.

24. Berne, B. J., and R. Pecora. 1976. Dynamic Light Scattering. J. Wiley & Son, New York.

25. Provencher, S. 1982. Contin: a general purpose constrained regularization program for inverting noisy linear algebric and integral equations. *Comput. Phys. Commun.* 27:213–227.

26. Provencher, S. 1982. A constrained regularization method for inverting data represented by linear algebraic or integral equations. *Comput. Phys. Commun.* 27:229–242.

27. Maulucci, G., M. De Spirito, G. Arcovito, F. Boffi, T. Congiu Castellano, and G. Briganti. 2005. Particle size distribution in DMPC vesicles solutions undergoing different sonication time. *Biophys. J.* 88:3545–3550.

28. Berliner, J. A., M. C. Territo, A. Sevanian, S. Ramin, J. A. Kim, B. Bamshad, M. Esterson, and A. M. Fogelman. 1990. Minimally modified low density lipoprotein stimulates monocyte endothelial interactions. *J. Clin. Invest.* 85:1260–1266.

29. Lin, M. Y., H. M. Lindsay, D. A. Weitz, R. C. Ball, R. Klein, and P. Meakin. 1990. Universal reaction-limited colloid aggregation. *Phys. Rev. A.* 41:2005–2020.

30. Brunelli, R., G. Mei, E. K. Krasnowska, F. Pierucci, L. Zichella, F. Ursini, and T. Parasassi. 2000. Estradiol enhances the resistance of LDL to oxidation by stabilizing apoB-100 conformation. *Biochemistry.* 39:13897–13903.

31. Pentikäinen, M. O., E. M. P. Lehtonen, and P. T. Kovanen. 1996. Aggregation and fusion of modified low density lipoprotein. *J. Lipid Res.* 37:2638–2649.

32. Öörni, K., M. Sneck, D. Brömme, M. O. Pentikäinen, K. A. Lindstedt, M. Mäyränpää, H. Aitio, and P. T. Kovanen. 2004. Cysteine protease cathepsin F is expressed in human atherosclerotic lesions, is secreted by cultured macrophages, and modifies low density lipoprotein particles in vitro. *J. Biol. Chem.* 279:34776–34784.

33. Hakala, J. K., K. Öörni, M. Ala-Korpela, and P. T. Kovanen. 1999. Lipolytic modification of LDL by phospholipase A2 induces particle aggregation in the absence and fusion in the presence of heparin. *Arterioscler. Thromb. Vasc. Biol.* 19:1276–1283.

34. Hevonoja, T., M. O. Pentikäinen, M. T. Hyvönen, P. T. Kovanen, and M. Ala-Korpela. 2000. Structure of low density lipoprotein (LDL) particles: basis for understanding molecular changes in modified LDL. *Biochim. Biophys. Acta.* 1488:189–210.

35. Brunelli, R., G. Greco, M. Barteri, E. K. Krasnowska, G. Mei, F. Natella, A. Pala, S. Rotella, F. Ursini, L. Zichella, and T. Parasassi. 2003. One site on the apoB-100 specifically binds 17-beta-estradiol and regulates the overall structure of LDL. *FASEB J.* 17:2127–2129.

36. Stefani, M., and C. M. Dobson. 2003. Protein aggregation and aggregate toxicity: new insights into protein folding, misfolding diseases and biological evolution. *J. Mol. Med.* 81:678–699.